

# Oxidation Behavior of Glassy Carbon in Acidic Electrolyte

Sakeb Hasan Choudhury,<sup>[a]</sup> Yuxiao Ding,<sup>\*[a, b]</sup> Youngmi Yi,<sup>[a]</sup> Christian Rohner,<sup>[c]</sup> Wiebke Frandsen,<sup>[c]</sup> Thomas Lunkenbein,<sup>[c]</sup> Mark Greiner,<sup>[a]</sup> Robert Schlögl,<sup>[a, c]</sup> and Saskia Heumann<sup>\*[a]</sup>

Glassy carbon is frequently used in electrochemical research due to its presumed robust electrochemical performance. Although it is widely utilized as a rotating disc electrode material, the modification of glassy carbon during electrocatalytic process is rarely emphasized or characterized. In this report, we investigated the structural modification of glassy carbon imparted by electrochemical oxidation in acidic media and compared the behavior with graphite. The functional groups generated from electrochemical oxidation in both electrodes possess similar electrochemical properties. However, above an oxidation potential of 1.8 V (vs. reversibly hydrogen

electrode), glassy carbon exhibits a lower electrochemical capacitance compared to graphite. We propose that the existence of electrochemically inactive species, originating from the non-graphitic portion of glassy carbon is attributed to such deterioration. Additionally, high resolution scanning electron microscopy (HR-SEM) and high-resolution transmission electron microscopy (HR-TEM) images corroborate how electrochemical oxidation prevails for glassy carbon electrodes at oxidative potentials. The overall analysis leads us to propose a corrosion mechanism for glassy carbon in acidic solution.

## Introduction

Carbon has been widely used in electrochemical applications as advanced electrodes due to the properties of high temperature resistance, low electrical resistance, relatively good chemical inertness and low cost.<sup>[1–4]</sup> Generally, it can play two different roles: catalytic site or support. For the catalytic part, some carbon materials exhibited good catalytic effects as metal-free catalysts for electrochemical reactions.<sup>[5–7]</sup> In some cases, oxygen-functionalized carbon materials were used as catalysts for oxidation evolution reaction (OER), in spite of carbon corrosion at oxidative potential.<sup>[8–10]</sup> In another part, carbon is often being used as catalyst support for those metal species to provide good electron transfer ability or to enhance the catalyst dispersity.<sup>[11,12]</sup> Commercial glassy carbon electrodes are often used to coat with different catalysts to study the performance


of the electrocatalysts. In this case, the carbon support is considered to be totally inert to the electrolytes and the applied potentials. However, regardless of whether it is being considered as a catalyst or support, in-situ changes to the carbon materials unavoidably happen because the standard potential of carbon oxidation is only 0.207 V vs. RHE (reversible hydrogen electrode).<sup>[1]</sup> Some changes of oxygen functionalization on carbon surfaces in electrolyte happen even without potential input.<sup>[13]</sup> Due to the complexity of the carbon surface chemistry, these changes are rarely considered. Yet, when carbon is used as a catalyst, there may actually be active sites for the catalytic process. Similarly, when carbon is used as a support, there may be in-situ formation of active C–O–metal species with supported electrocatalyst. Hence, neglecting to consider the chemical species formed on the carbon surface can lead to misunderstandings of the relative catalytic mechanisms.


Comparing with other carbon materials, glassy carbon (GC) normally shows higher stability in electrochemical applications, thus being used as commercial rotating disc electrode.<sup>[14,15]</sup> It is a type of non-graphitic carbon structure, formed by pyrolysis of certain polymer or resin precursor. The existence of crosslinks in the early stage of preparation can be anticipated, but their persistence is very unlikely after annealing at temperatures above 2000 °C, which are necessary to achieve “partial graphitization”.<sup>[16–18]</sup> These stiff structural parts, or crosslinks, formed during partial graphitization impede the movement of graphite ribbons along each other. The presence of crosslinks in GC is what distinguishes it from its parent graphitic structure even up to nano-metric level. The unique structure of the GC obviously causes different electrochemical behaviors with other carbon structures. Although in previous work, the degradation of a GC electrode has been reported by electrochemical oxidation at high anodic potentials but the instability issue of GC in electrochemical applications is still not well considered.

[a] Dr. S. H. Choudhury, Dr. Y. Ding, Dr. Y. Yi, Dr. M. Greiner, Prof. Dr. R. Schlögl, Dr. S. Heumann  
Department of Heterogeneous Reactions  
Max Planck Institute for Chemical Energy Conversion  
Stiftstrasse 34–36, 45470 Mülheim an der Ruhr, Germany  
E-mail: yuxiaoding@licp.cas.cn  
saskia.heumann@cec.mpg.de

[b] Dr. Y. Ding  
Lanzhou Institute of Chemical Physics  
Chinese Academy of Sciences  
No. 18, Tianshu Middle Road, Lanzhou, China, ZIP: 730000

[c] Dr. C. Rohner, W. Frandsen, Dr. T. Lunkenbein, Prof. Dr. R. Schlögl  
Inorganic Chemistry  
Fritz-Haber-Institute of the Max Planck Society  
Faradayweg 4-6, 14195 Berlin, Germany

 Supporting information for this article is available on the WWW under <https://doi.org/10.1002/celec.202200637>

 © 2022 The Authors. ChemElectroChem published by Wiley-VCH GmbH. This is an open access article under the terms of the Creative Commons Attribution License, which permits use, distribution and reproduction in any medium, provided the original work is properly cited.

That is because those degradations are only visible after long term electrochemical treatments, when it shows clear structure changes on the carbon surface.<sup>[19]</sup> In fact, all the corrosion processes start from the formation of oxygen functional groups on the carbon surface. Oxygen functional groups on the carbon surface plays a very important role in electrochemistry. In a recent work, it was demonstrated that the so-called metal free carbon catalyst for OER is caused by the formation of C–O–Fe species between specific oxygen functional groups on carbon surface and the iron impurities in the electrolyte.<sup>[20]</sup> Therefore, determining the functionalization of the GC electrode in different applications is essential for understanding the real mechanism of the supported catalysts and designing appropriate electrodes.<sup>[21–23]</sup>

For achieving a precise overview, in this work a primary analysis was carried out on the pristine structure of the glassy carbon followed by an electrochemical treatment in acidic electrolyte with the range of OER potential. Both graphitic and non-graphitic parts of the glassy carbon were considered and compared with an only graphitic graphite material. Graphite (Gr) and GC received the same electrochemical treatment. The treated samples were subsequently characterized by numerous tools to analyze and compare how the oxidative potentials affect the complete and partially graphitized carbon. The discussion was aimed to develop fundamental understanding of structural modification of glassy carbon which is the main topic of interest.

## Results and Discussion

Different bonding motifs among carbon atoms initiate vast difference in its final structure and properties. Planar networks of  $sp^2$  hybridized carbon atoms can be stacked one over another by  $\pi$ – $\pi$  interaction to form a thermodynamically stable structure: graphitic carbon. GC is a partial graphitic material. The widely accepted model of glassy carbon is depicted as entangled ribbon-like crystalline graphite layers embedded in the matrix of structural components termed as crosslinks.<sup>[24,25]</sup> High resolution transmission electron microscopy (HR-TEM) images (Figure 1a) taken from GC lamella (Figure S1) show a consolidation of three-dimensional (3D) graphitic ribbons and non-graphitic connecting agent. The observable maximum length (red arrow line,  $L_a$ ) of this graphitic ribbon is 10–15 nm and the stacking width (white arrow line,  $L_c$ ) is about 3–4 nm which categorize its structural attributions similar to non-graphitizing carbon. The non-graphitic part is encapsulated within the stacked and curved graphitic layers to build up a closed pore-like arrangement, shown with green circles in Figure 1b. A possible structural model of the glassy carbon based on the model given by Jenkins and Kawamura is shown in Figure 1c.<sup>[26]</sup> The model mainly shows two parts: graphitic layers and the connection part between those graphitic layers (in the green cycle). This intricate structure of glassy carbon is analyzed by Raman spectroscopy and a comparison with a fully graphitized structure (graphite) can be found in Figure 1d. The significantly larger peak areas of D and D' bands in the glassy

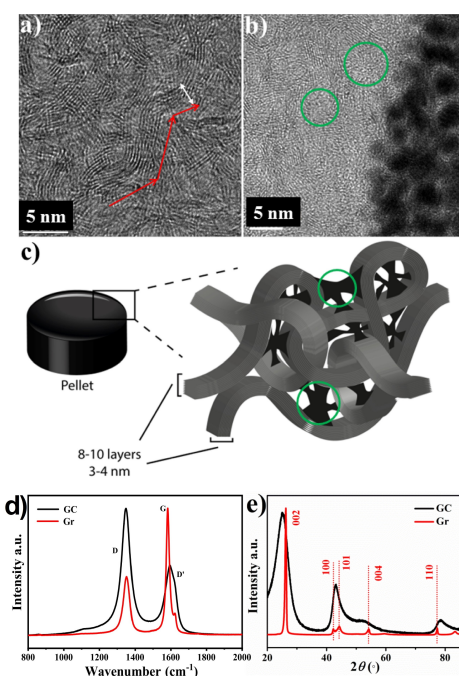


**Figure 1.** (a) Microscopic images of a glassy carbon lamella. The pattern and branching of graphitic crystallites throughout the whole structure is indicated by red arrows. Due to three dimensional structures, the  $L_a$  is difficult to determine. The maximum length that could be determined was 15 nm. The observed highest stacking ( $L_c$ ) was found to be around 3.75 nm shown with the white arrow. (b) Green circles indicate the non-graphitic entities surrounded by stacked graphitic layers. Dark Pt particles seen at the right side is the result from the lamella preparation. (c) An improvised structural model of glassy carbon based on the model given suggested by Jenkins and Kawamura. (d) Comparison of Raman spectra of pristine graphite and glassy carbon. (e) XRD spectra of pristine glassy carbon and graphite substrates.

carbon can be directly correlated to the short-range stacking order and defective structure.<sup>[27–29]</sup> Similarly, the broad peaks in the X-ray diffraction (XRD) pattern (Figure 1e) of glassy carbon reflects the randomly oriented nanostructured crystalline phases of glassy carbon.<sup>[30,31]</sup>

Electrochemical treatments were performed in acidic media to investigate the bulk structural changes of both carbon electrodes. The chronoamperometry (CA) current profiles for potentials between 1.2 and 2.4  $V_{RHE}$  of the two different carbon electrodes in 0.1 M  $H_2SO_4$  electrolyte are shown in Figure 2a, b. During CA, the current densities result from both carbon oxidation and water oxidation. In glassy carbon as well as the graphite electrodes, a low steady state current density is observed at low CA potentials up to 1.5  $V_{RHE}$ . However, when a potential of 1.8  $V_{RHE}$  is applied, an increase of the current density is observed within the 10 minutes in the case of the glassy carbon. Up to 1.8  $V_{RHE}$ , both samples show relatively low current, which mainly arises from the carbon oxidation process, as no obvious bubble formation was observed. At higher potentials, such as 2.1 and 2.4  $V_{RHE}$  significant currents can be observed, that can be related to the oxidation of the electrode. Before they reach a steady state, a small peak is observable. It appears that this peak shift closer towards the beginning of CA with increasing applied potential. This indicates that the

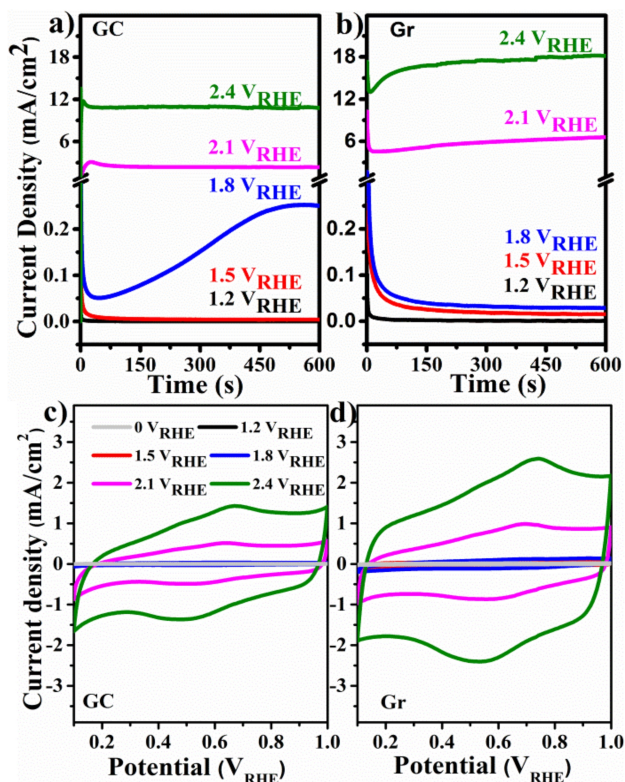


**Figure 2.** The CA current profiles of (a) a glassy carbon and (b) a graphite electrode at different oxidation potentials in acidic electrolyte are presented. CV between 0.1 and 1  $V_{RHE}$  after 10 min CA scans at different potentials of (c) glassy carbon and (d) graphite electrodes.

commencement of electrochemical process requires shorter activation time when the oxidation potential is raised. Within the 600 seconds of measurement time, the current shows a slight decrease, which might be caused by physical detachment of the unstable connection part of the GC. In the case of Gr, the CA current continuously decreases over time at low potentials (1.2–1.8  $V_{RHE}$ ). This might be caused by the saturation of the oxidative sites of the Gr edges. At higher potentials the opposite trend is found, and the currents increase over time (2.1 and 2.4  $V_{RHE}$ ). Compared to the curved graphitic structures of the GC, the Gr has more exposed edges. The high potentials have better oxidative ability, which can produce more defective sites. Therefore, it can exhibit higher and increasing currents in this range compared to GC.

Cyclic voltammograms (CV) were recorded between the hydrogen and oxygen evolution reaction potential of 0.1 and 1  $V_{RHE}$  for GC and Gr as shown in Figure 2 c and d, respectively. The electrochemical capacity is represented by the charge of the CV. The electrochemical oxidation of the carbon electrodes lead to the formation of a hydrated and oxygen functionalized surface layer, which causes an increase in electrochemical capacity in both cases. Gr shows a tendency towards higher current densities and capacities compared to GC due to the mentioned more exposed edges. Considering the Faradaic current peaks of the CV, it can be interpreted that the functional groups emanating from electrochemical oxidation in both

electrodes possess similar electrochemical properties. These observations are in agreement with our previous work.<sup>[19]</sup> Measurements in different pH ranges were also carried out and it can be seen that the pH has an enormous influence on the degradation mechanism, but the comparison is not part of this main work (Figure S2–S5).

Figure 3 shows the corresponding selected area electron diffraction (SAED) patterns and the HR-TEM images recorded from the pristine and the treated GC. The HR-TEM investigations were performed on the lamellae cut from the GC pellets (Figure S1). The dark granular particles in the side of the images (Figure 3c, f, i) are Pt deposited on the surface of the GC electrodes during lamella preparation; therefore, the interfaces seen here are the surfaces of the glassy carbon pellets. The TEM image of the pristine GC shows a homogeneous contrast (Figure 3b), whereas the electrochemically treated GCs each show two different contrast regions (Figure 3e, h). A brighter region near the surface Pt layer and a darker region of the bulk. The brighter region extends to about 83 nm, and 1240 nm away from the surface for the cases of 1.8  $V_{RHE}$  and 2.4  $V_{RHE}$  treatment, respectively. The brighter regions reflect a decreased material density and structural order as a result of the electrochemical treatment. The dimension of the affected depth also correlates to the potential of the electrochemical oxidation of the glassy electrode surface. The SAED patterns were recorded in the cases of pristine GC and 1.8  $V_{RHE}$  on the darker regions (Figure 3a, d). The image taken in the case of GC treated at 2.4  $V_{RHE}$  was from the brighter region (Figure 3g). Here, the relatively more diffuse pattern from the brighter region indicating a more amorphous structure of the surface. Comparing the HR-TEM images (Figure 3c, f, i), the pristine sample shows graphitic as well as amorphous components, whereas

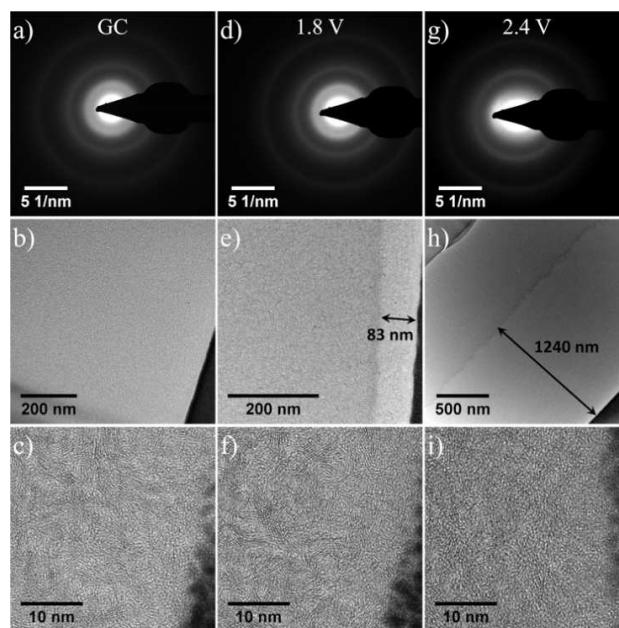


**Figure 3.** The corresponding SAED pattern and HR-TEM images from the near surface regions of (a–c) pristine glassy carbon, (d–f) glassy carbon treated with 1.8  $V_{RHE}$  and (g–i) 2.4  $V_{RHE}$  in acidic electrolyte.

the sample treated at 1.8 V<sub>RHE</sub> shows an increased proportion of graphitic components. On the other hand, the sample treated at high potentials shows mainly amorphous structures. The length and stacking of the graphitic crystallites are significantly reduced after oxidizing at 2.4 V<sub>RHE</sub> as seen in Figure 3i.

The HR-TEM and SAED results suggest that sequential removal of non-graphitic parts occurred in the GC samples treated at 1.8 V<sub>RHE</sub> and after treatment with 2.4 V<sub>RHE</sub>, additional decomposition of the graphitic portions take place.

As evident from Figure 3, the structural disruption contributed from electrochemical treatment in acidic media is very much confined to the surface region. It is reflected in the results of XRD where no significant difference could be detected after electrochemical treatment for either GC and Gr samples (Figure 4a, b).

Raman spectroscopy is one of the most commonly used characterization techniques to analyze carbon materials.<sup>[34–37]</sup> In the present study, the investigated pellet samples were analyzed by Raman spectroscopy using a 532 nm laser with a variable power. As the laser treatment also has influence on the carbon structures and the resulting Raman spectra, different laser powers were used for the samples to exclude the influence (Figure S6).

Raman spectra of Gr treated at different potentials (Figure 4d) show an increase in the intensity of the D and D' bands or decrease of the G band with increasing oxidation potential, while maintaining the same peak width. The determined G

band positions (Figure 4e) and intensity ratios I(D)/I(G) (Figure 4f) increase with applied potentials. They follow the transformation from graphite to nanocrystalline graphite as described by Ferrari et al.<sup>[27]</sup> A change of the virtual slope is noticed at the higher potentials, this correlates with the distinct changes that could be observed in the CV spectra assigned to the electrochemical oxidation.

In the case of GC, the determined trends of the G band positions (Figure 4e) and intensity ratios I(D)/I(G) (Figure 4f) cannot be directly correlated to the amorphization trajectory of the three-stage model from Ferrari of graphite. When first considering the G position, one observes a shift to smaller wavenumbers of the G position of the samples that were treated with low potentials. This indicates an increase in graphitic components and correlates with the HR-TEM observations. Applying higher potentials, lead to a shift of the G position to higher wavenumbers which correlates with the transition towards a nanocrystalline carbon structure. That means the graphitic parts are electrochemically oxidized at higher potentials. Considering the I(D)/I(G) ratios, the decreasing values with increasing potential do not fit to stage I like the G positions but to stage II, i.e., the transition of nanocrystalline carbon into amorphous carbon. We assume that the effects observed for GC in Raman superimpose and that the G position is more dominated by the graphitic components while the signal intensity ratios are influenced by both the graphitic and amorphous components of the GC. Thus, based on the I(D)/I(G) ratios, one can observe that the proportion of amorphous components in the carbon increases.

In addition, an increase in signal intensity and broadening at the regions of the D and G bands can be also caused by molecular structures that are formed during the oxidation process. Molecular vibration and stretching modes arise at:  $\nu(\text{aromatic C-C})$  (1600–1580, 1500, 1400 cm<sup>-1</sup>),  $\nu(\text{C=C})$  (1900–1500 cm<sup>-1</sup>),  $\nu(\text{C=O})$  (1820–1680 cm<sup>-1</sup>),  $\delta(\text{CH}_2 \text{ and } \text{CH}_3)$  (1470–1400 cm<sup>-1</sup>) and  $\nu(\text{C-O-C})$  (1150–1060 cm<sup>-1</sup>).

Scanning electrode microscopy (SEM) was utilized to examine the surface morphology of the treated electrodes. In Figure 5, the comparison of SEM images from different glassy carbon samples are arranged. Comparing the SEM image of the pristine sample (Figure 5a) with the 1.8 V<sub>RHE</sub> treated sample, only slight modifications of the surface are visible (Figure 5c). The scratches seem a little more pronounced but this effect

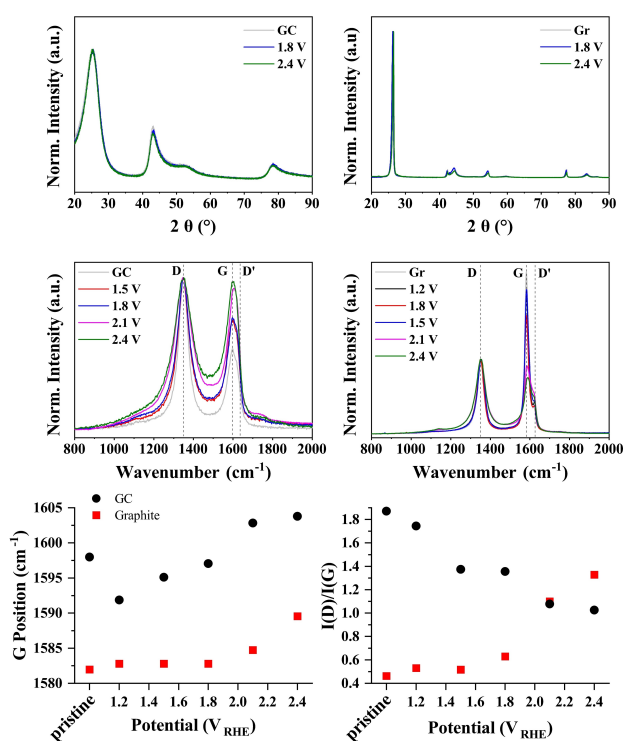


**Figure 4.** (a, b) XRD patterns of the pristine and treated (a) GC and (b) Gr samples at different potentials. (c, d) Raman spectra of the pristine and treated (c) GC and (d) Gr samples at different potentials. (e) Position of the G band and (f) I(D)/I(G) ratio of GC and Gr in dependence of the applied potentials.

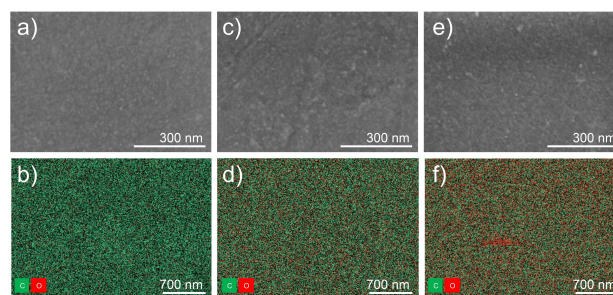


**Figure 5.** SEM and EDX-mapping images of the pristine and treated GC samples. (a, b) pristine GC, (c, d) treated with potential 1.8 V<sub>RHE</sub>, and (e, f) treated with 2.1 V<sub>RHE</sub>.

may also be due to the contrast. The comparison with the sample treated at 2.1  $V_{\text{RHE}}$  (Figure 5e) also reveals no additional modification. The energy dispersive X-ray spectroscopy (EDX)-mapping images on the other hand show a clear trend with increasing potential. For the pristine glassy carbon sample, no obvious functionality (oxygen content; red color) is observed from the EDX mapping (Figure 5b). For the electrochemically treated glassy carbon samples (Figure 5d, f), the comparison of red color contrast in the EDX mapping shows a distinct increase in oxygen content.

The SEM images of pristine Gr substrate show that the surface is a combination of holes and smooth areas (Figure 6a). In the image, electrostatic charging appears as bright features at the graphitic edges. After oxidizing with 1.8  $V_{\text{RHE}}$ , the surface exhibits flake-like morphology of graphitic layers with fewer smooth areas (Figure 6c). This display of edge features is representative of electrochemical exfoliation and can be clearly distinguished from the pristine graphite.<sup>[38]</sup> In the SEM image of graphite oxidized with 2.1  $V_{\text{RHE}}$ , it can be found that a number of plateaus start to emerge which look similar to the smooth areas of the pristine graphite (Figure 6e). In addition, the bright contrast from the graphitic edge is also visible here. The observed flat plateau of the treated graphite samples is understood as the result of exfoliation which accompanies the electrochemical oxidation process. Although the SEM images of the different Gr samples exhibit significant morphological differences, their EDX-Mapping images show no obvious change of the content of the oxygen functionality. The reason could be that the saturation of electrochemical oxidation of the graphitic edges. Comparing the Gr and GC samples, it appears that the curved 3-dimensional structure of the GC is more robust against electrochemical degradation than the Gr. The exfoliation of the single graphene sheets seems to be hindered when they are entwined with each other.

We utilized X-ray photoemission spectroscopy (XPS) to investigate the functional groups produced on the carbon materials during the electrochemical oxidation. The C1s spectra of electrochemically oxidized graphite and glassy carbon samples are shown in Figure 7a and b. For both carbon materials, the measured spectra of electrochemically treated samples are plotted with the spectra of a pristine sample. The differential spectra are also shown at the bottom. Based on literature, the positions of different carbon-oxygen components

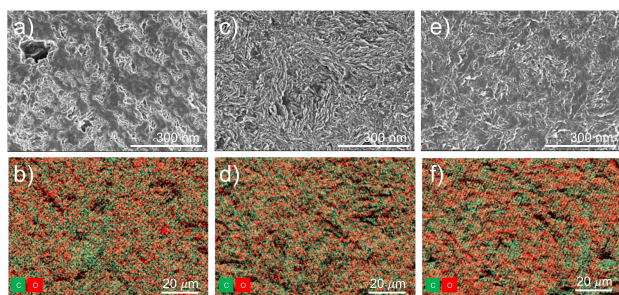


**Figure 6.** SEM and EDX-mapping images of the pristine and treated Gr samples. (a, b) pristine Gr, (c, d) treated with potential 1.8  $V_{\text{RHE}}$ , and (e, f) treated with 2.1  $V_{\text{RHE}}$ .

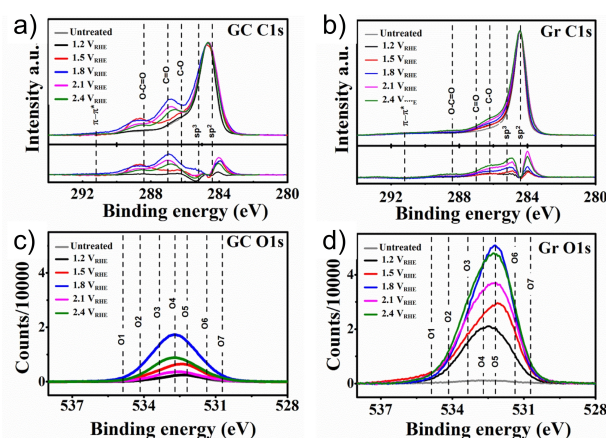


**Figure 7.** (a, b) Comparison of C1s spectra of the pristine and oxidized (a) GC and (b) Gr with different potential are shown. The vertical dash lines represent the contribution of  $sp^2$ ,  $sp^3$  bonded carbon and different carbon oxygen functional groups. (c, d) Comparison of O1s spectra of the pristine and oxidized (c) GC and (d) Gr with different potential are shown.

of a graphitic system are assigned and labeled with vertical dash lines.<sup>[39]</sup> It can be observed that the spectral contributions from the  $sp^3$  component and different oxygen-derived functional groups increase with higher applied potentials, in case of graphite samples (Figure 7b). The glassy carbon samples treated at low potential, such as 1.2 and 1.5  $V_{\text{RHE}}$ , also show an increase of functional groups. But the C1s peak shape changes when the potential was increased above 1.5  $V_{\text{RHE}}$ . We can also identify that the peak shape and area does not follow the reference vertical line positions related to the functional groups. The two features around  $\sim 287$  and 288.5 eV become more pronounced in the C1s spectra of glassy carbon when the applied potential was 1.5  $V_{\text{RHE}}$  or higher. These features can be attributed to a combination of functional group and possibly electrostatic charging. We expect differential charging might arise in glassy carbon from the lack of long-range graphitic domains, as seen from the TEM images. These high-binding-energy C1s features were not observed in any of the graphite samples. From the data, it can be clearly recognized that the amount of oxygen-containing functional groups had drastically increased with electrochemical treatment. In both carbon materials, carbon-oxygen functional groups increase when oxidation potential increases. Considering the oxygen atomic percentage of both carbon materials in pristine condition, it is apparent that graphite develops more carbon-oxygen functional groups through electrochemical treatment than glassy carbon. The trend was also observed in the electrochemical data.

O1s spectra recorded for graphite electrodes is not suitable for peak fitting because the line-shape is built from many broad peaks that are too close to one another to be resolvable. Nonetheless, we have indicated on Figure 7c and d showing at which binding energies various oxygen species would be expected.<sup>[40]</sup>

To characterize and identify different functional groups on the glassy carbon materials, thermo-gravimetric mass spectroscopy (TG-MS) measurements were performed.<sup>[41]</sup> From the

data, no conclusive changes could be assigned. This can be explained due to the fact that TG-MS is a bulk sensitive characterization technique and the electrochemical oxidation takes place on the glassy carbon surfaces (Figure S7). Furthermore, we performed in situ temperature programmed XPS (TPD-XPS) measurements with GC treated at  $2.4 V_{RHE}$ . The recorded C1s and O1s spectra are shown in Figure S8. In figure S8, changes can be observed in both C1s and O1s spectra with increasing temperature. It indicates that volatile functional groups decompose during the in-situ annealing of electrochemically oxidized glassy carbon. We can speculate that this volatile functional groups can be correlated to the presence of electrochemically modified non-graphitic portion of glassy carbon.

## Conclusion

We have investigated changes that occur in glassy carbon and graphite after electrochemical treatment within the OER potential window. Although the chronoamperometric treatments were performed for a relatively short period (10 minutes), significant structural changes of the carbons were observed. In the case of glassy carbon, it can be observed that with increasing applied potential, the concentration of oxygen functional groups increases (EDX, XPS). Similarly, the capacity of the oxidized GC increases with increasing potential as it can be observed in the CV measurement. Nevertheless, the microscopic structure of the GC remains almost unchanged, no significant differences can be observed in the SEM images nor in the XRD patterns. However, detailed observation using HR-TEM and SAED shows that structural changes still occur at the surface where contact with the electrolyte took place. In accordance with the Raman data, we can propose a structural decomposition mechanism of glassy carbon that proceeds as follows. At a relatively low potential of  $1.8 V_{RHE}$ , amorphous components are initially decomposed which leads to an apparent increase in graphitic components. At a higher potential of  $2.4 V_{RHE}$  a further decomposition of the graphitic part of the GC occurs (Scheme 1).

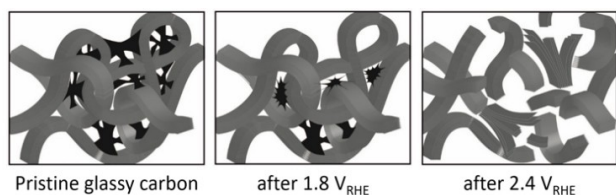
In comparison, Graphite shows a clear macroscopic structural change even at the relatively low potential. An exfoliation behavior of graphite is known from literature can be observed here. This is accompanied by the direct decomposition of the graphitic parts.

In summary, therefore, it can be claimed that graphitic carbon structures exhibit higher stability under electrochemical

reaction conditions than amorphous structures. In addition, the stability of the carbon-based electrodes also depends on the three-dimensional network of the graphitic entities. From our results, it is evident that a planar arrangement of relatively large graphitic layers is less stable than multiple tagliatelle-like graphitic ribbons that are twisted within themselves. Whether this effect depends only on the applied potential or is also changed by a longer reaction time will be investigated in a next study. However, as a conclusive remark, electrochemical measurements performed for example with a supporting GC disc electrode, should in any case take into account that they potentially be altered by the applied potentials, which can affect the performance and stability of the deposited catalyst.

## Experimental Section

For ensuring reproducibility and homogeneity of our experiment we purchased mirror polished glassy carbon disks (SIGRADUR G type) with a dimension of 5 mm thickness and 10 mm diameter from HTW (Hochtemperatur-Werkstoffe GmbH, Germany). Graphite pellets of same dimension purchased from Mateck were polished with a very fine sand paper (3000) to expose a silvery surface since conventional scotch tape peeling leaves behind contamination. Prior to the electrochemical treatment, the pellets were sonicated in Millipore water to eliminate surface impurities imparted by the polishing process. A stationary three electrode system controlled by an EC-lab-BioLogic VMP3 potentiostat was equipped for treating these pellets, where a Pt wire, a standard calomel and a Hg/HgO electrode were used as the counter and reference electrode. The electrolytes used for all the experiment are 0.1 M  $H_2SO_4$  (pH = 1). CA as well as CV measurements were performed. Electrochemically prepared functional groups were further characterized by XPS with a Specs GmbH Phoibos 150 NAP-XPS instrument using Al K $\alpha$  (1486.6 eV) as the photon source. The spectrometer was calibrated by setting the Au4f $_{7/2}$  binding energy of sputter cleaned gold foil to 83.98 eV. The spot size for all measurements was 350 microns with a takeoff angle of 90°. The core level spectra of carbon and oxygen were taken with a step width of 0.05 eV and pass energy of 20 eV to ensure a high resolution. The sample was heated via illuminating the back side of the sample holder with an infrared laser. The temperature was measured via a type K thermocouple spot welded to the stainless-steel sample holder. Utilizing the highest safe laser power, XPS measurements could be performed at maximum 1240 K (~960°C). A Thermo-Fisher Scientific DXR Raman laser of 532 nm wavelength and power from 0.1 to 5 mW was utilized to record the Raman spectra of the samples. Surface morphology of the treated pellets was studied through SEM. The electron microscope images were captured on a Hitachi S-4800 field emission scanning electron microscope, working in the kV range 0.1 to 30. For our work, typical morphology studies are undertaken at low voltages 1.5 kV and a relatively close working distance of 3 mm. The EDX analysis data were detected with a Bruker EDX System applying a SDD (silicon drift detector). EDX yielded a spatially resolved elemental composition for tracing the surface as well as sub surface modification. The working distance for detecting x-rays was optimized to 10 mm. TEM was conducted with a Cs-corrected FEI Titan 80–300 microscope with acceleration voltage of 80 kV coupled with a Gatan Ultrascan 1000 camera. For HR-TEM analysis, lamellae were prepared from every pellet using focused ion beam with a FEI HELIOS Nanolab G3UC. A STA 449 F3 Jupiter VR QMS4 from Netzsch with an argon gas flow of 70 mL/min was used for the TG-MS analysis. The applied heating rate was 20 K/min between the isothermal steps for avoiding overheating. During the isothermal



**Scheme 1.** Proposed degradation process of glassy carbon.

steps, the decomposed functional groups are captured in the mass spectroscopy as CO and CO<sub>2</sub>.

## Acknowledgements

The authors thank the Max Planck Society for funding. Open Access funding enabled and organized by Projekt DEAL.

## Conflict of Interest

The authors declare no conflict of interest.

## Data Availability Statement

The data that support the findings of this study are available from the corresponding author upon reasonable request.

**Keywords:** carbon-based electrode · carbon degradation · carbon stability · electrocatalysis · OER

- [1] K. Kinoshita, *Carbon: electrochemical and physicochemical properties*, John Wiley Sons, New York, United States, 1988.
- [2] D. S. Su, S. Perathoner, G. Centi, *Chem. Rev.* **2013**, *113*, 5782–5816.
- [3] C. Tang, M. M. Titirici, Q. Zhang, *J. Energy Chem.* **2017**, *26*, 1077–1093.
- [4] M. M. Titirici, R. J. White, N. Brun, V. L. Budarin, D. S. Su, F. del Monte, J. H. Clark, M. J. MacLachlan, *Chem. Soc. Rev.* **2015**, *44*, 250–290.
- [5] Y. Lin, K.-H. Wu, Q. Lu, Q. Gu, L. Zhang, B. Zhang, D. Su, M. Plodinec, R. Schlögl, S. Heumann, *J. Am. Chem. Soc.* **2018**, *140*, 14717–14724.
- [6] Y. Lin, Z. Liu, L. Yu, G. R. Zhang, H. Tan, K. H. Wu, F. Song, A. K. Mechler, P. P. M. Schleker, Q. Lu, B. Zhang, S. Heumann, *Angew. Chem. Int. Ed.* **2021**, *60*, 3299–3306; *Angew. Chem.* **2021**, *133*, 3336–3343.
- [7] Y. Lin, Q. Lu, F. Song, L. Yu, A. K. Mechler, R. Schlögl, S. Heumann, *Angew. Chem. Int. Ed.* **2019**, *58*, 8917–8921; *Angew. Chem.* **2019**, *131*, 9010–9014.
- [8] A. M. El-Sawy, I. M. Mosa, D. Su, C. J. Guild, S. Khalid, R. Joesten, J. F. Rusling, S. L. Suib, *Adv. Energy Mater.* **2016**, *6*, 1501966.
- [9] X. Lu, W.-L. Yim, B. H. R. Suryanto, C. Zhao, *J. Am. Chem. Soc.* **2015**, *137*, 2901–2907.
- [10] Y. Zhang, X. Fan, J. Jian, D. Yu, Z. Zhang, L. Dai, *Energy Environ. Sci.* **2017**, *10*, 2312.
- [11] P. Dungen, M. Greiner, K.-H. Böhm, I. Spanos, X. Huang, A. A. Auer, R. Schlögl, S. Heumann, *J. Vac. Sci. Technol. A* **2017**, *36*, 01A126.
- [12] N. Alexeyeva, E. Shulga, V. Kisand, I. Kink, K. Tammeveski, *J. Electroanal. Chem.* **2010**, *648*, 169–175.
- [13] S. Reiche, R. Blume, X. C. Zhao, D. S. Su, E. Kunkes, M. Behrens, R. Schlögl, *Carbon* **2014**, *77*, 175–183.
- [14] A. Dekanski, J. Stevanović, R. Stevanović, B. Z. Nikolić, V. M. Jovanović, *Carbon* **2001**, *39*, 1195–1205.
- [15] M. G. Sullivan, B. Schnyder, M. Bärtsch, D. Allia, C. Barbero, R. Imhof, R. Kötz, *J. Electrochem. Soc.* **2000**, *147*, 2636–2643.
- [16] G. M. Jenkins, K. Kawamura, *Nature* **1971**, *231*, 175.
- [17] P. J. F. Harris, *Crit. Rev. Solid State Mater. Sci.* **2005**, *30*, 235–253.
- [18] K. Jurkiewicz, M. Pawlyta, D. Zygadlo, D. Chrobak, S. Duber, R. Wrzalik, A. Ratuszna, A. Burian, *J. Mater. Sci.* **2018**, *53*, 3509–3523.
- [19] Y. Yi, G. Weinberg, M. Prenzel, M. Greiner, S. Heumann, S. Becker, R. Schlögl, *Catal. Today* **2017**, *295*, 32–40.
- [20] Y. Ding, Q. Gu, A. Klyushin, X. Huang, S. H. Choudhury, I. Spanos, F. Song, R. Mom, P. Dungen, A. K. Mechler, R. Schlögl, S. Heumann, *J. Energy Chem.* **2020**, *47*, 155–159.
- [21] R. L. Borup, J. R. Davey, F. H. Garzon, D. L. Wood, M. A. Inbody, *J. Power Sources* **2006**, *163*, 76–81.
- [22] M. Cai, M. S. Ruthkosky, B. Merzougui, S. Swathirajan, M. P. Balogh, S. H. Oh, *J. Power Sources* **2006**, *160*, 977–986.
- [23] K. Kinoshita, *Carbon, Electrochemical and Physical Properties*, John Wiley & Sons, Chichester, New York, Brisbane **1988**, *92*, 1060–1060.
- [24] P. J. F. Harris, *Int. Mater. Rev.* **1997**, *42*, 206–218.
- [25] P. J. F. Harris, *Philos. Mag.* **2004**, *84*, 3159–3167.
- [26] G. M. Jenkins, K. Kawamura, *Nature* **1971**, *231*, 175–176.
- [27] A. Ferrari, J. Robertson, *Phys. Rev. B: Condens. Matter Mater. Phys.* **2000**, *61*, 14095–14107.
- [28] M. A. Pimenta, G. Dresselhaus, M. S. Dresselhaus, L. G. Cancado, A. Jorio, R. Saito, *Phys. Chem. Chem. Phys.* **2007**, *9*, 1276–1290.
- [29] F. Tuinstra, J. L. Koenig, *J. Chem. Phys.* **1970**, *53*, 1126–1130.
- [30] L. A. Pesin, *J. Mater. Sci.* **2002**, *37*, 1–28.
- [31] A. F. Craievich, *Mater. Res. Bull.* **1976**, *11*, 1249–1255.
- [32] I. Mochida, R. Ohtsubo, K. Takeshita, H. Marsh, *Carbon* **1980**, *18*, 117–123.
- [33] W. Ruland, B. Smarsly, *J. Appl. Crystallogr.* **2002**, *35*, 624–633.
- [34] P. Dungen, M. Prenzel, C. Van Stappen, N. Pfänder, S. Heumann, R. Schlögl, *Materials Sciences and Applications* **2017**, *8*, 628–641.
- [35] M. S. Dresselhaus, G. Dresselhaus, R. Saito, A. Jorio, *Physics Reports* **2005**, *409*, 47–99.
- [36] A. C. Ferrari, J. Robertson, *Phys. Rev. B* **2000**, *61*, 14095–14107.
- [37] A. M. Rao, E. Richter, S. Bandow, B. Chase, P. C. Eklund, K. A. Williams, S. Fang, K. R. Subbaswamy, M. Menon, A. Thess, R. E. Smalley, G. Dresselhaus, M. S. Dresselhaus, *Science* **1997**, *275*, 187–191.
- [38] H. S. Choo, T. Kinumoto, Y. Iriyama, T. Abe, Z. Ogumi, *ECS Transactions*, **2007**, *11*, 1, 1003–1011 (<https://iopscience.iop.org/article/10.1149/1.2781013/pdf>).
- [39] T. I. T. Okpalugo, P. Papakonstantinou, H. Murphy, J. McLaughlin, N. M. D. Brown, *Carbon* **2005**, *43*, 153–161.
- [40] H. Li, Determination of Oxygen Functionality on Highly Oriented Pyrolytic Graphite (HOPG), Dissertation, Frei Universität Berlin, **2012**.
- [41] P. Dungen, R. Schlögl, S. Heumann, *Carbon* **2018**, *130*, 614–622.

Manuscript received: June 8, 2022

Revised manuscript received: August 4, 2022

Accepted manuscript online: September 2, 2022